ISSN: 2458-8989

Natural and Engineering Sciences

NESciences, 2026, 11 (2): 59-75 doi: 10.28978/nesciences.262005

Survey and Classification of Desert Soils in Karbala Governorate Using Smart Agricultural Technology

Rana S. Abdulsada*, Abdulhalim A. Sulaima

Department of Soil and Water Resources Sciences, College of Agricultural Engineering Sciences, University of Baghdad, Baghdad 10071, Iraq.

Abstract

This study aimed to evaluate the efficiency of smart agriculture technologies, particularly unmanned aerial vehicles (UAVs), in surveying and classifying desert soils in Karbala Governorate, Iraq. The study area is located in the western desert of Karbala between longitudes 43°51′29″–43°59′08″ E and latitudes 32°34′13″–32°35′41″ N, covering approximately 10,000 ha. High-resolution aerial images were acquired using a UAV at an altitude of 200 m and compared with Sentinel-2 satellite imagery acquired on 21 April 2024 during the same period. Geometric correction was applied to both datasets, and the images were used as base maps for soil survey and classification at the soil series level. Supervised and unsupervised classification techniques were applied to the UAV and satellite images. UAV imagery achieved a spatial resolution of 0.04 × 0.04 m, whereas Sentinel-2 imagery provided a resolution of 10 × 10 m, demonstrating the superior spatial accuracy of the UAV data. The results revealed that compared with conventional satellite-based approaches, UAV-based soil surveys offer higher accuracy, faster implementation, and lower costs. A total of twelve distinct soil series were identified and mapped, all belonging to the Aridisols soil order. This study confirms the effectiveness of UAV technology as a reliable tool for detailed desert soil surveys and classification in arid environments.

Keywords:
Unmanned Aerial Vehicles (UAVs); Smart Agriculture Technologies; Soil Survey; Remote Sensing; Desert Soils

Available online: 02/06/2026

Introduction

Smart agriculture represents a modern agricultural approach that relies on advanced technologies to increase crop productivity, optimize land and water use, reduce production costs, and improve resource management while supporting food security and sustainable development. In recent years, smart agriculture has played a vital role in addressing climate change challenges through the integration of remote sensing technologies with unmanned aerial vehicles (UAVs).

Remote sensing is considered one of the most effective tools for soil survey and classification, as it enables the acquisition, processing, and analysis of spatial data from various sensors to generate high-resolution thematic maps. The accuracy of remote sensing techniques varies according to soil physical and chemical properties, spectral indicators, salinity levels, surface color, and spatial extent (Abdel-Qader et al., 2023). In parallel, geographic information systems (GIS) and satellite imagery have been widely used to evaluate desert lands, and practical solutions have been proposed to mitigate desertification processes (Abdulsada, 2020). The advancement of GIS and remote sensing technologies has significantly reduced the challenges associated with traditional soil survey methods by providing

*Corresponding Author: Rana S. Abdulsada, E-mail: rana.abd2207p@coagri.uobaghdad.edu.iq

comprehensive spatial coverage of previously unstudied areas and establishing integrated geodatabases for soil information (Dawod, 2013). Compared with conventional approaches, remote sensing offers faster data acquisition, higher accuracy, repeated monitoring capability, and extensive area coverage (Lekka et al., 2024).

Unmanned aerial vehicles (UAVs), commonly referred to as drones, have emerged as powerful tools for farm monitoring, precision agriculture, and sustainable land management because of their ability to capture very high-resolution imagery at relatively low operational costs (Wadod & Mohammed, 2023). UAVs have been successfully applied to monitor crop variability during growth and production stages using vegetation indices derived from spectral wavelengths (Wheib et al., 2024). Their cost-effectiveness and ability to provide detailed spatial information make them highly competitive with other remote sensing platforms (Wijayanto et al., 2023). Moreover, remote sensing techniques have been effectively employed to predict crop nutrient requirements, including phosphorus availability, demonstrating their reliability as active tools for agricultural decision-making (Jasim et al., 2020). These technologies have also facilitated soil investigations in remote or inaccessible areas, offering a low-cost alternative for mapping the spatial distribution of soil properties (Al-Sarajati, 2020).

UAVs can be integrated with conventional satellite imagery to achieve higher spatial accuracy, faster data processing, and improved temporal monitoring at lower operational costs (Ndehedehe, 2021). Owing to their high spatial resolution and flexible flight parameters, UAVs are considered optimal platforms for detailed aerial imaging in agricultural and soil studies (Tamouridou et al., 2017). Flight altitude plays a critical role in image quality, where higher altitudes provide broader coverage with lower spatial resolution, whereas lower altitudes offer finer resolution at the expense of coverage area (Torres-Sánchez et al., 2014; Hamad & Suliman, 2021). Recent studies in Iraq have demonstrated the successful application of UAV imagery for soil surveys and agricultural mapping, enabling accurate discrimination between cultivated and uncultivated soils, vegetation cover, and soil surface features, often surpassing satellite imagery in detail and accuracy (Al-Jubouri et al., 2023; Sadiq, 2023). Furthermore, the integration of machine learning and artificial intelligence techniques has enhanced soil mapping efficiency by reducing financial, temporal, and labor requirements (Abdelelah & Wheib, 2025). UAV-based imagery has proven particularly effective in revealing variations in soil surface appearance, which reflect underlying differences in soil physical and chemical properties (Al-Hemoud et al., 2020).

Materials and Methods

Study Area

This study was conducted in the western desert of Karbala Governorate, which extends toward the road leading to Hisn Al-Akhadir, approximately 76 km southwest of Karbala city (Figure 1). The total study area covers approximately 10,000 ha. The region is characterized by an arid climate, low annual rainfall, high evapotranspiration rates, sparse natural vegetation, and dominant desert landforms. The terrain is generally flat to gently undulating, making it suitable for detailed soil surveys and remote sensing–based investigations (Abdulsada, 2020; Al-Sarajati, 2020).

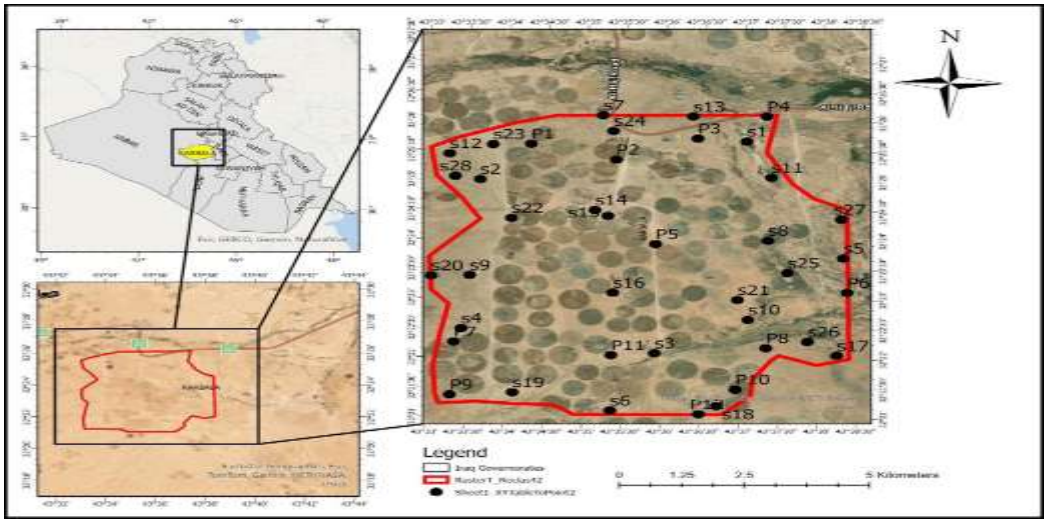

Figure 1. Study area

Aerial and satellite image acquisition

High-resolution aerial images were acquired using a DJI Mavic 2 Pro unmanned aerial vehicle (UAV) equipped with a 20-megapixel RGB camera capable of capturing 4K images. UAV flights were conducted at an altitude of 200 m under stable atmospheric conditions to minimize image distortion and ensure optimal radiometric quality (Tamouridou et al., 2017). The resulting spatial resolution of the UAV imagery was approximately 0.04 × 0.04 m, enabling detailed identification of soil surface features.

In parallel, multispectral satellite imagery was obtained from the Sentinel-2A sensor operated by the European Space Agency (ESA), providing a spatial resolution of 10 × 10 m. The Sentinel-2 image was acquired on 21 April 2024, which coincided with the UAV data acquisition period to ensure temporal consistency between datasets (ESA, 2023).

Image Preprocessing and Geometric Correction

Geometric correction and preprocessing of the UAV and satellite images were performed using ArcGIS and Global Mapper software. Ground control points (GCPs) were used to georeference the imagery and correct spatial distortions, thereby minimizing errors in area, distance, and scale measurements (Lillesand et al., 2015). The corrected images were mosaicked and used as base maps for soil interpretation, classification, and mapping.

Image Classification and Interpretation

Both the UAV and Sentinel-2 images were subjected to supervised and unsupervised classification techniques. Image interpretation relies on variations in surface color, texture, drainage patterns, vegetation cover, and microtopographic features, which are commonly used indicators for soil boundary delineation in arid environments (Dawod, 2013; Abdel-Qader et al., 2023). The integration of UAV and satellite data enhanced classification accuracy by combining high spatial resolution with broader spatial coverage (Ndehedehe, 2021).

Field Survey and Soil Sampling

Reconnaissance field surveys were conducted to validate image interpretation and assess soil variability across the study area. Survey routes and sampling locations were determined on the basis of UAV imagery, satellite data, landform characteristics, and natural vegetation indicators (Soil Survey Staff, 2017).

The free lance soil survey method was adopted because of its flexibility and suitability for large desert areas with heterogeneous soil conditions (Denton & Whitney, 1992). A total of 12 representative pedons were excavated to represent the central concept of the identified soil series. The morphological descriptions included horizon depth, color (Munsell soil color charts), structure, consistency, carbonate accumulation, and gypsum occurrence.

Laboratory Analyses

Soil samples from each horizon were air-dried, crushed, and sieved through a 2-mm mesh prior to laboratory analysis. Standard analytical methods were applied to determine the following soil properties:

- Soil texture (hydrometer method; Gee & Bauder, 1986)
- Soil reaction (pH) in a 1:1 soil–water suspension (Page et al., 1982)
- Electrical conductivity (ECe) for salinity assessment (Richards, 1954)
- Organic matter content was determined using the Walkley–Black method (Nelson & Sommers, 1982)
- Calcium carbonate (lime) content
- Gypsum content
- Cation exchange capacity (CEC) (Chapman, 1965)
- Exchangeable calcium and magnesium
- Exchangeable sodium percentage (ESP)

These analyses supported soil classification and facilitated the interpretation of spectral responses observed in UAV and satellite imagery (Al-Hemoud et al., 2020).

Results and Discussion

Digital processing of the satellite images

The Sentinel-2 satellite scene covering the study area was first identified and subset to match the spatial extent of the UAV imagery. A series of digital preprocessing steps, including radiometric enhancement and geometric refinement, were applied prior to visual interpretation and classification. These processes

improved image clarity and contrast, enhanced surface feature discrimination, and facilitated the accurate delineation of soil and land-cover units. Similar preprocessing approaches have been widely recommended to improve thematic map accuracy in arid and semiarid regions (Lillesand et al., 2015; Abdel-Qader et al., 2023).

Unsupervised classification

Unsupervised classification was applied to both UAV aerial imagery and Sentinel-2 satellite imagery to explore natural spectral groupings without prior training data. The results showed a high degree of consistency with field survey observations, with only minor discrepancies compared with ground truth data. The UAV imagery produced 15 spectral classes, whereas the satellite scene yielded 13 classes (Figures 2 and 3).

The greater number of classes derived from UAV imagery reflects its finer spatial resolution, which enables better discrimination of subtle variations in soil surface characteristics, vegetation cover, and landform features. Similar findings were reported by Tamouridou et al. (2017) and Al-Jubouri et al. (2023), who demonstrated that high-resolution UAV data improve the detection of soil and land cover heterogeneity in arid landscapes.

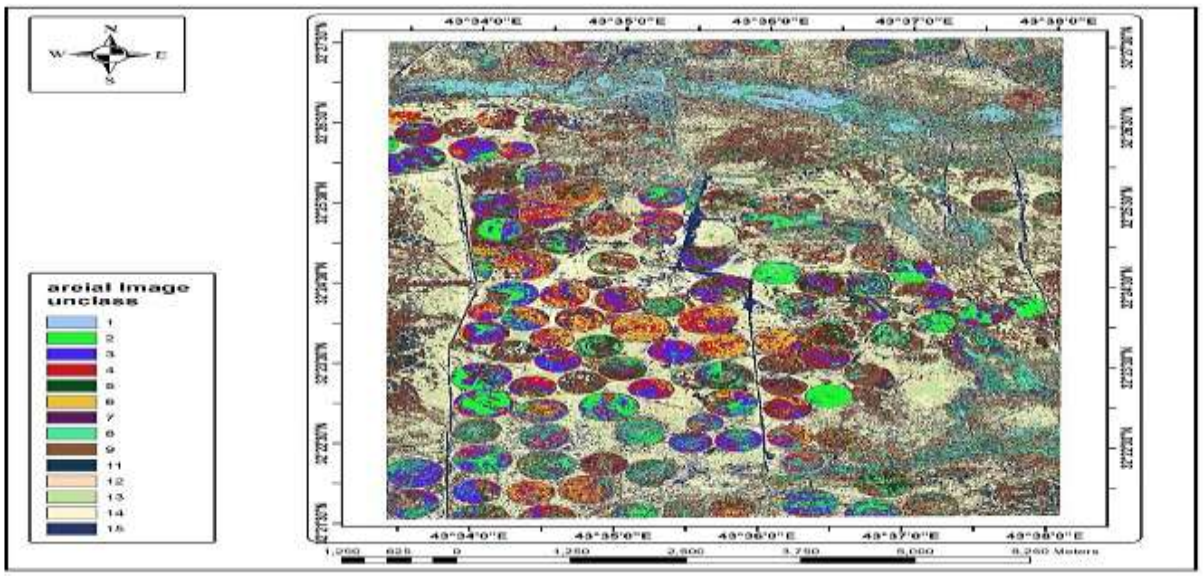

Figure 2. Unsupervised classification of aerial images

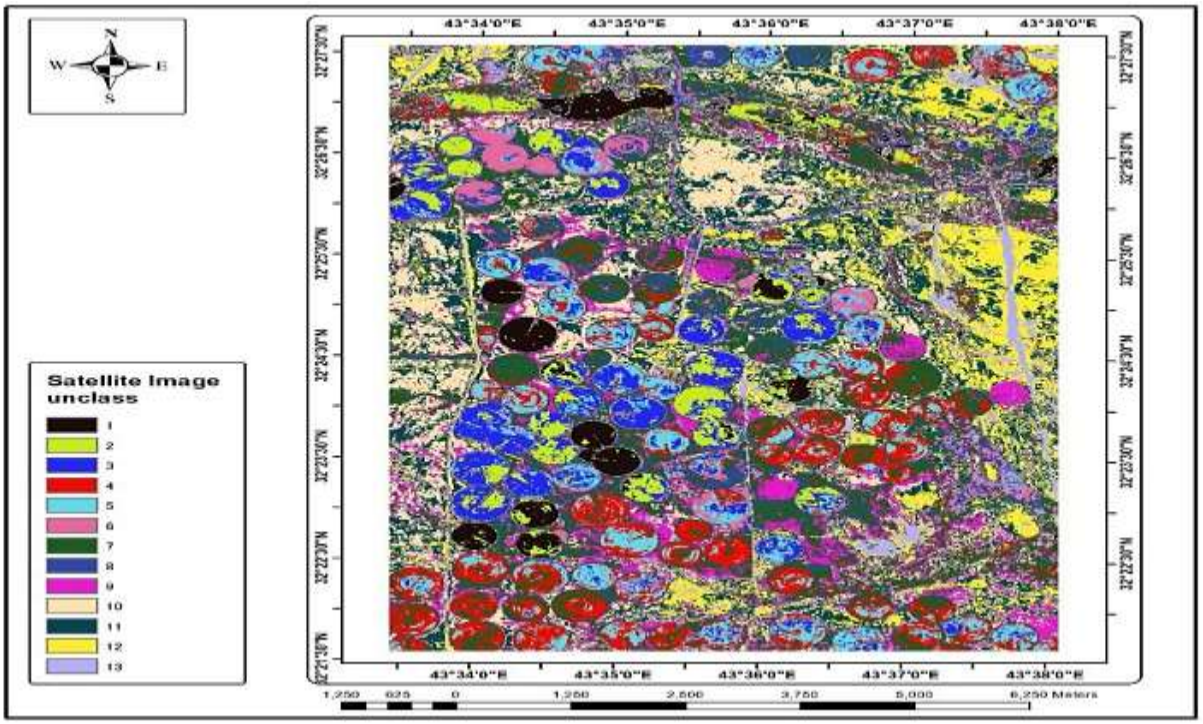

Figure 3. Unsupervised classification of the satellite scene

Supervised classification

Supervised classification was performed using carefully selected training sites that represented the dominant soil series and land use types within the study area. Spectral signatures were extracted on the basis of field-verified locations to ensure classification reliability. The results revealed 10 distinct classes in the UAV imagery and 7 classes in the Sentinel-2 imagery, encompassing soil series and other land use categories (Figures 4 and 5).

The reduced number of classes in the satellite imagery can be attributed to spectral mixing effects caused by larger pixel sizes, which limit the ability to distinguish small or heterogeneous surface features. In contrast, UAV imagery provided more detailed and accurate class separation, particularly for soil-related features. These results align with those of previous studies that highlighted the superiority of UAV-based supervised classification over medium-resolution satellite data for detailed soil mapping (Ndehedehe, 2021; Sadiq, 2023).

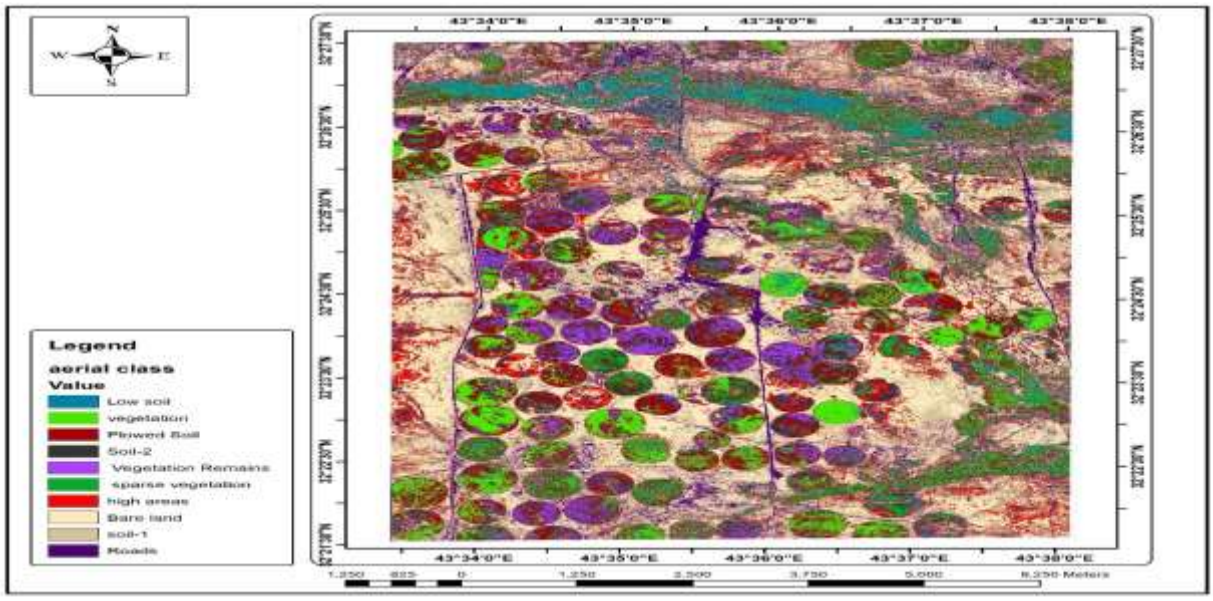

Figure 4. Supervised classification of aerial imagery

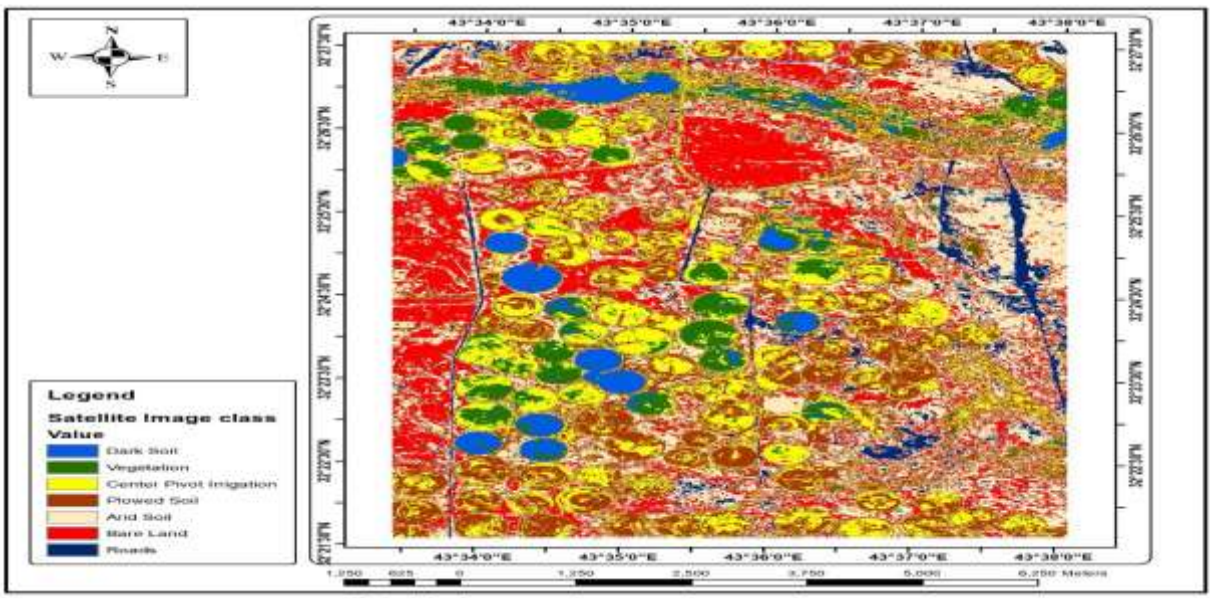

Figure 5. Supervised classification of the satellite scene

Comparison of spatial resolution between the aerial image and the satellite scene

Spatial resolution differences between the UAV and Sentinel-2 imagery were quantified using pixel (cell) size as a key indicator. UAV imagery, with a spatial resolution of approximately 0.04 × 0.04 m, revealed fine-scale details of land cover and soil features that were not detectable in the Sentinel-2 imagery, which has a resolution of 10 × 10 m (Figures 6 and 7).

Supervised classification results, supported by field verification, revealed ten land cover classes in the UAV imagery, including trees, crops, herbs, soil types, archaeological soils, roads, elevated areas, barren soils, ploughed soils, and scattered vegetation. In contrast, the Sentinel-2 imagery was limited to broader classes, such as center-pivot irrigated fields, barren soils, roads, ploughed soils, and arid soils.

These differences are primarily attributed to pixel size, as smaller pixels reduce spectral mixing and enhance feature discrimination, leading to higher spatial accuracy (Torres-Sánchez et al., 2014; Hamad & Suliman, 2021). These findings confirm that UAV imagery is particularly effective for detailed soil surveys and land cover mapping in desert environments, where surface variability occurs at very fine spatial scales. Similar conclusions were reported by Al-Hemoud et al. (2020) and Abdelelah and Wheib (2025), who emphasized the role of high-resolution imagery and advanced analytical techniques in improving soil mapping accuracy.

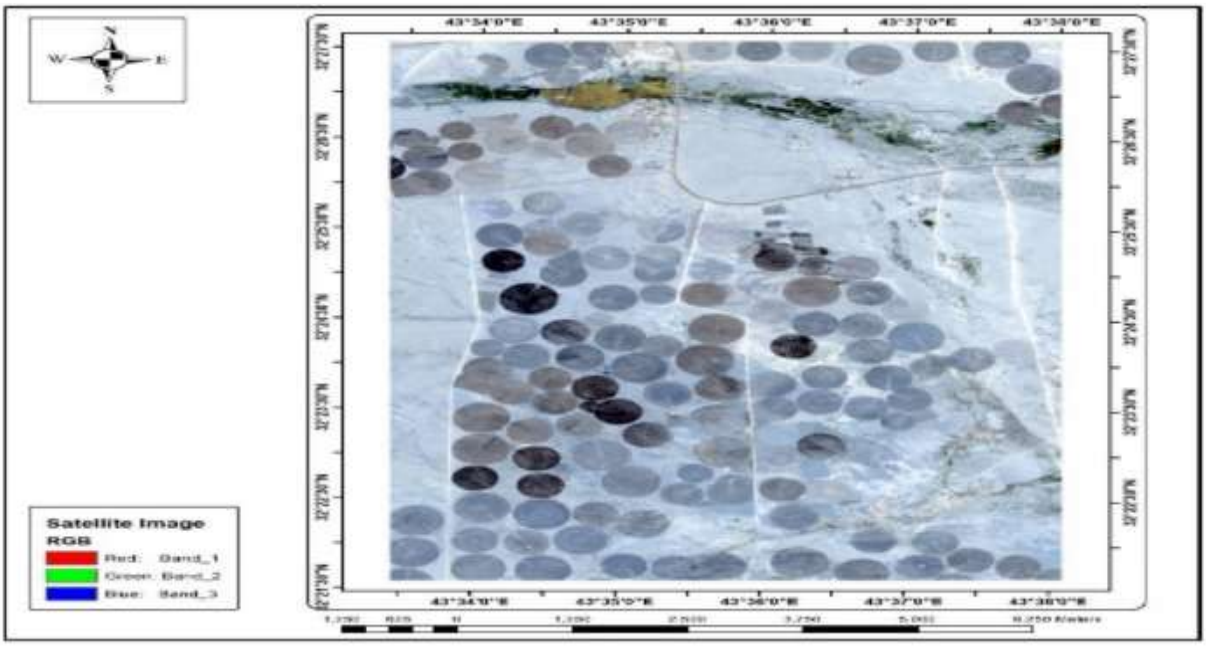

Figure 6. The satellite scene

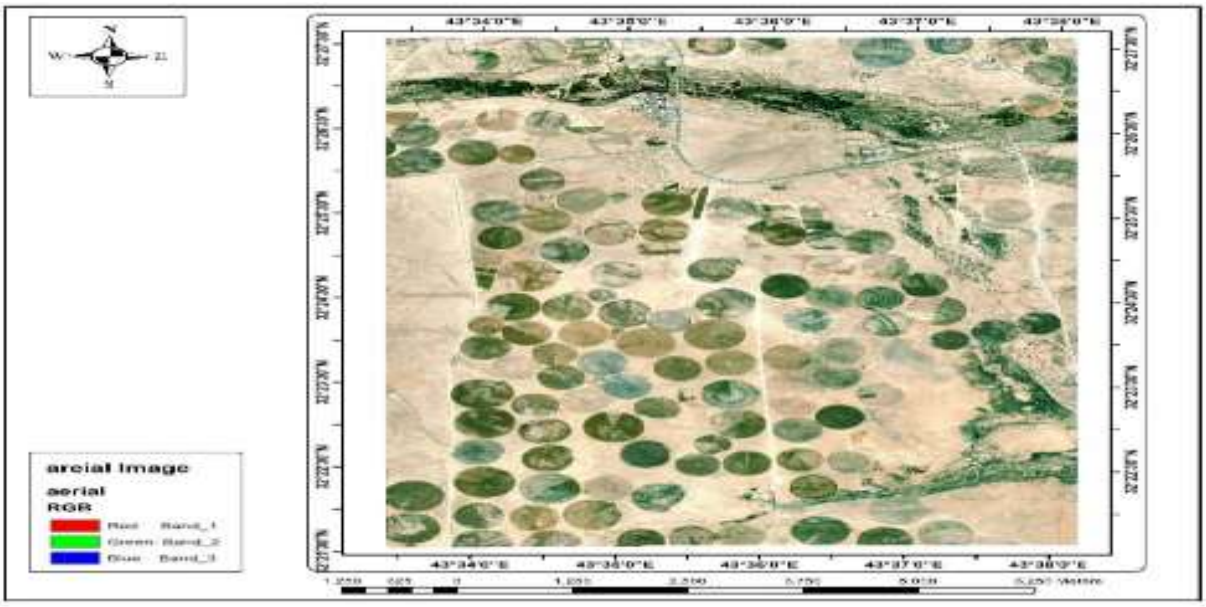

Figure 7. Aerial image

Implications for Desert Soil Surveys

The integration of UAV imagery with satellite data and field observations provided a robust framework for accurate soil survey and classification. UAV-based mapping proved superior in terms of spatial detail, classification accuracy, and flexibility, whereas satellite imagery contributed broader spatial context. This complementary approach enhances the reliability of soil series delineation and supports

sustainable land management and smart agriculture applications in arid regions.

Soil texture

The results indicated that the sand content ranged from 75.2–95.6%, while the silt content ranged from 0.4–15.6%, and the clay content ranged from 2.8–14.4% across all the study sites. Physical analyses of soil separates revealed that the sand content was generally high throughout the study area. This is attributed to depositional processes typical of desert soils, in addition to soil formation resulting from aeolian (wind-blown) additions and deposits (Al-Jubouri and Wheib, 2020).

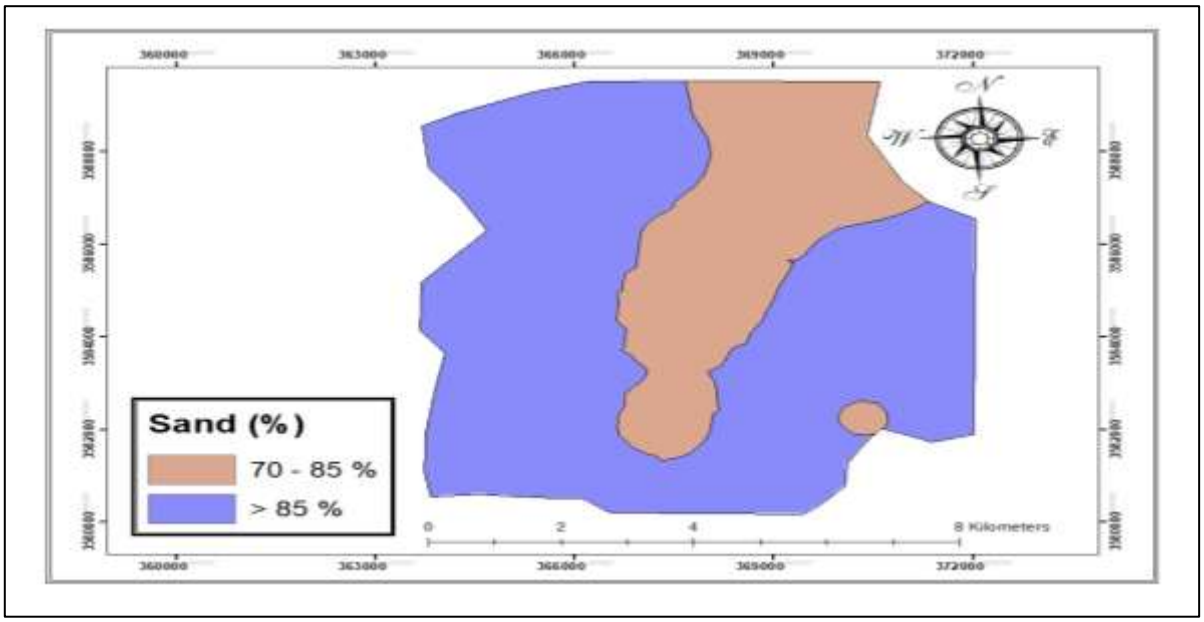

Figure 8. Spatial distribution of sand separates in the AP horizon of the study area

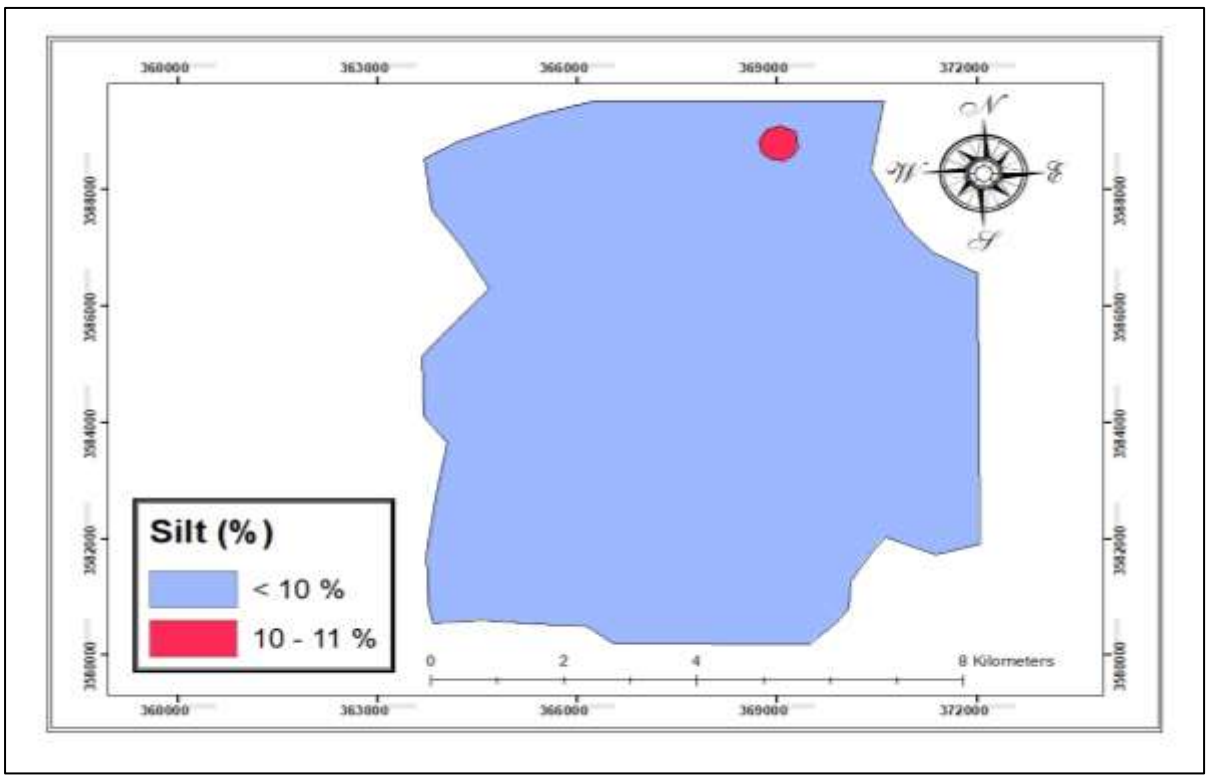

Figure 9. Spatial distribution of silt separates in the AP horizon of the study area

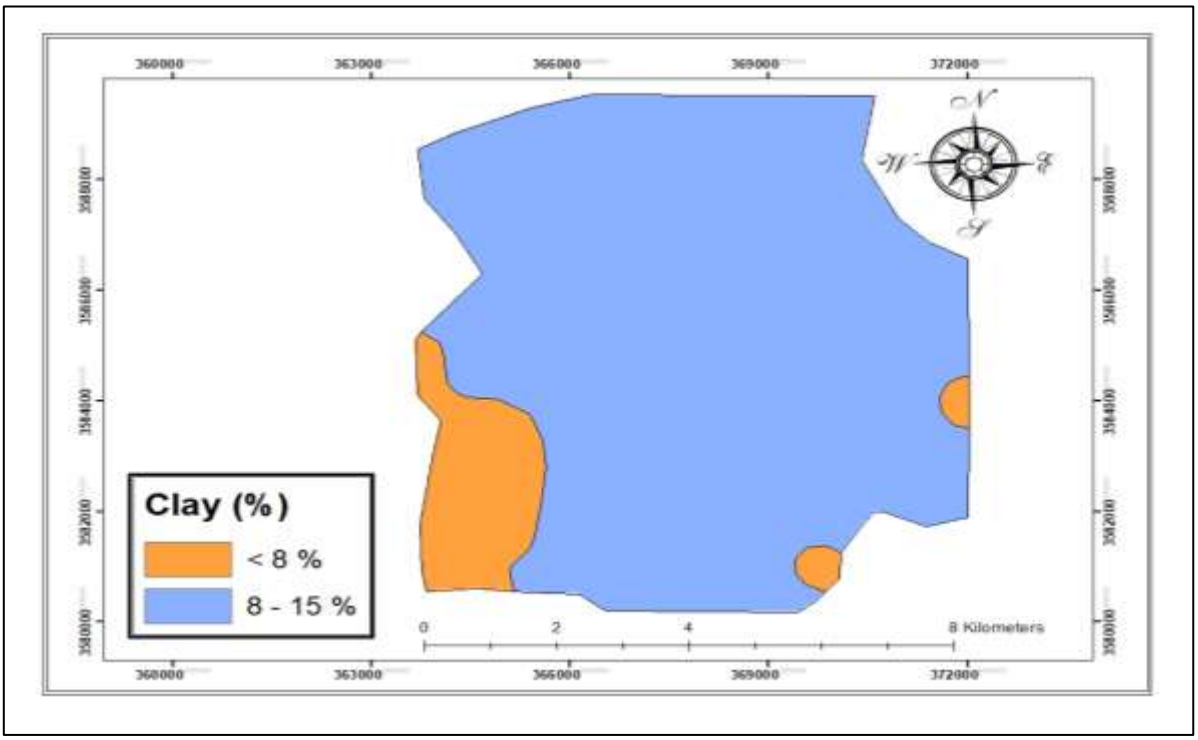

Figure (10). Spatial distribution of clay separates in the Ap horizon of the study area

Soil reaction (pH)

As shown in Table (2), the soil pH values ranged between 7.0 and 8.4, with the highest value recorded at 8.4 and the lowest at 7.0. The increase in soil alkalinity is primarily due to the high content of calcium carbonate, whereas a higher gypsum content has the opposite effect, leading to reduced pH values.

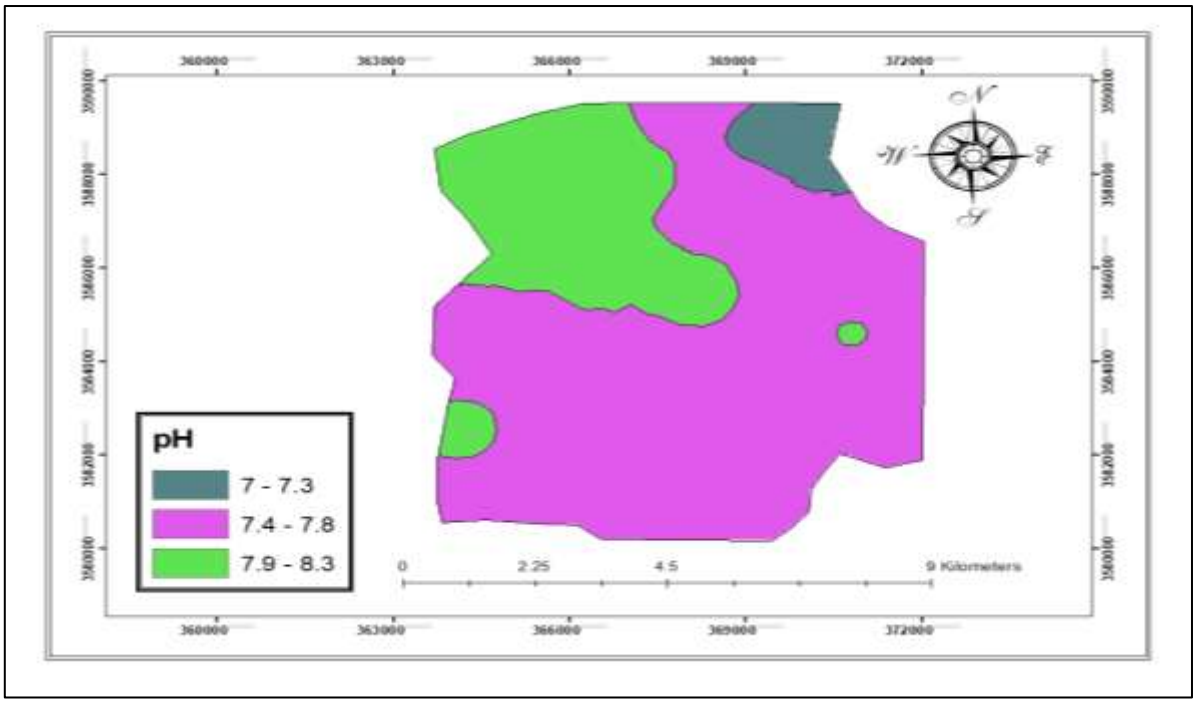

Figure 11. Spatial distribution of soil reaction (pH) in the study area

Table 1. Mechanical analysis and soil texture of the horizons of the study pedons

Pedon	Horizon	Sand %	Silt %	Clay %	zA
1	Ap	89.2	1.6	9.2	Loamy Sand
	Cy	87.2	7.2	5.6	Loamy Sand
	Cky	86.8	0.8	12.4	Loamy Sand
	C_1	85.6	2.4	12.0	Loamy Sand

2	Ap	88.4	0.4	11.2	Loamy Sand
	Cy_1	93.2	0.8	6.0	Sand
	Cy_2	95.6	1.2	3.2	Sand
	Cy_3	94.4	1.6	4.0	Sand
3	Ap	76.4	10.4	13.2	Sandy Loam
	C_1	92.4	1.2	6.4	Sand
	Cky	92.0	0.8	7.2	Sand
	C_2	83.6	6.8	9.6	Loamy Sand
4	Ap	82.0	4.0	14.0	Sandy Loam
	Cy_1	84.0	5.6	10.4	Loamy Sand
	Cy_2	75.2	13.6	11.2	Sandy Loam
	Cy_3	80.8	5.2	14.0	Sandy Loam
5	Ap	82.0	3.6	14.4	Sandy Loam
	Cy_1	82.0	4.0	14.0	Sandy Loam
	Cy_2	82.0	4.0	14.0	Sandy Loam
	Cy_3	82.0	3.6	14.0	Sandy Loam
6	Ap	93.2	0.4	6.4	Sand
	Cy_1	81.6	7.2	11.2	Sandy Loam
	Cy_2	81.9	6.4	11.7	Sandy Loam
	C_1	81.6	15.6	2.8	Loamy Sand
7	Ap	89.6	6.0	4.4	Loamy Sand
	C1	91.6	6.4	2.0	Sand
	Cy	88.0	5.6	6.4	Loamy Sand
	C2	91.2	6.0	2.8	Sand
8	Ap	83.6	2.8	13.6	Sandy Loam
	Cy	93.4	2.0	4.6	Sand
	Cky	93.4	1.0	5.6	Sand
	Ck	90.8	3.6	5.6	Sand
9	Ap	93.6	1.2	5.2	Sand
	Ck_1	85.4	3.8	10.8	Loamy Sand
	Ck_2	80.0	6.4	13.6	Sandy Loam
	Ck_3	92.8	2.0	5.2	Sand
10	Ap	90.0	4.4	5.6	Sand
	Ck	92.0	1.2	6.8	Sand
	Cky_1	86.0	4.0	10.0	Loamy Sand
	Cky_2	75.2	11.6	13.2	Sandy Loam
11	Ap	83.2	3.2	13.6	Sandy Loam
	Ck_1	82.8	2.8	14.4	Sandy Loam
	Ck_2	82.8	5.2	12.0	Sandy Loam
	Ck_3	92.8	1.6	5.6	Sand
12	Ap	85.2	0.8	14.0	Sandy Loam
	Cky_1	79.6	8.0	12.4	Sandy Loam
	Cky_2	89.2	1.2	9.6	Loamy Sand
	Cky_3	82.4	6.0	11.6	Loamy Sand

Soil salinity (EC)

The results of electrical conductivity, presented in Table (2), showed variable values across the study area, ranging from 0.46 to 51.6 dS m^{-1}. Soil electrical conductivity is influenced by several factors, such as texture, parent material, rainfall rate, and management practices. The dominance of coarse textures, combined with the arid climate and irregular management practices, contributed to elevated salinity levels reaching 51.6 dS m^{-1} (4). This directly affects productivity, particularly when salt concentrations become high in soils. According to Pessoa et al. (2022). The expansion of agriculture into areas not previously cultivated also contributes to increased salt accumulation (Mohammed and Suliman, 2023).

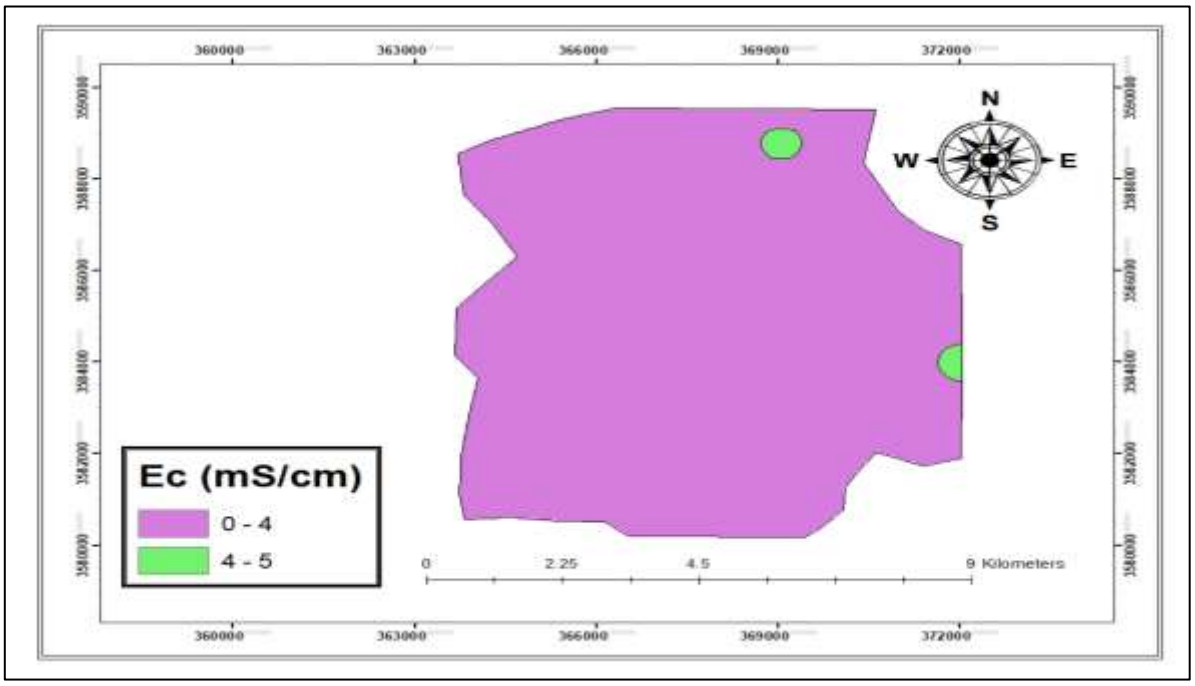

Figure 12. Spatial distribution of soil salinity in the study area

Exchangeable sodium percentage (ESP)

The results in Table (2) indicate that the ESP ranged between 6.4% and 8.3%. The relatively low ESP values in some soils can be attributed to the high calcium carbonate and magnesium contents, whereas higher ESP values reflect increased sodium content in these soils.

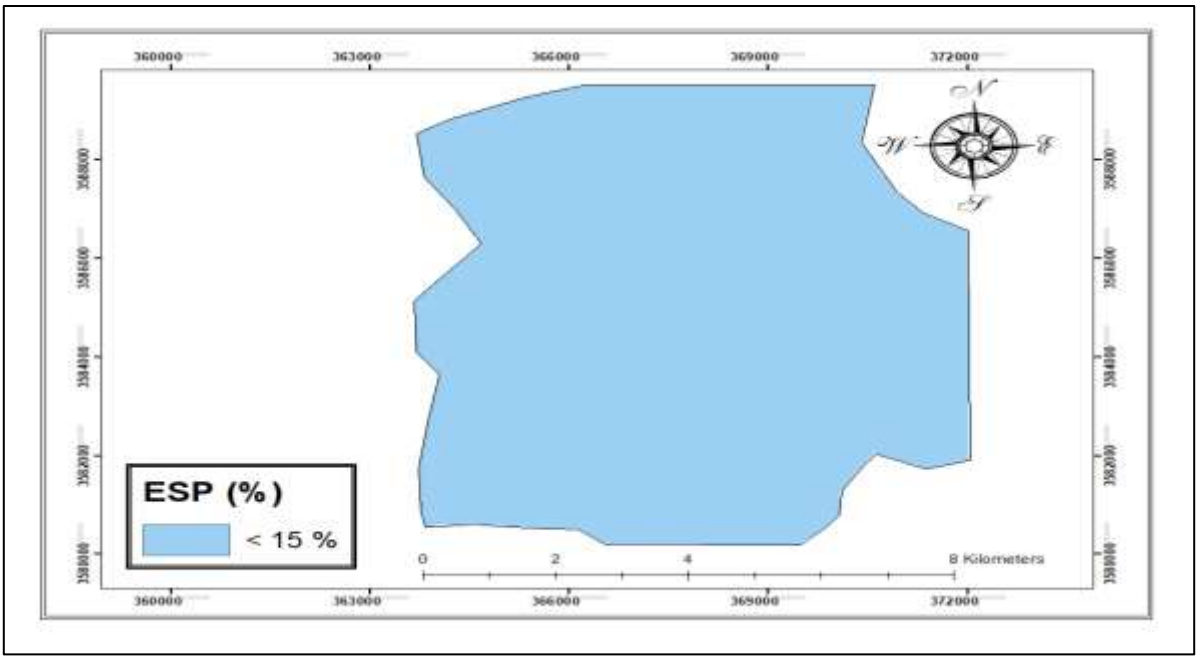

Figure 13. Exchangeable sodium percentage (ESP)

Cation exchange capacity (CEC)

As shown in Table (2), the CEC values ranged between 3.2 and 9.36 cmol (+) kg^{-1}. The reduction in the CEC is associated with high proportions of sand and calcium carbonate, which tend to coat soil particles, in addition to the accumulation of gypsum in desert soils. According to the inverse relationship between the CEC and calcium sulfates, as the sulfate content increases at the expense of other components, such as organic matter and clay, the overall cation exchange capacity decreases (Abbas and Wahib, 2022).

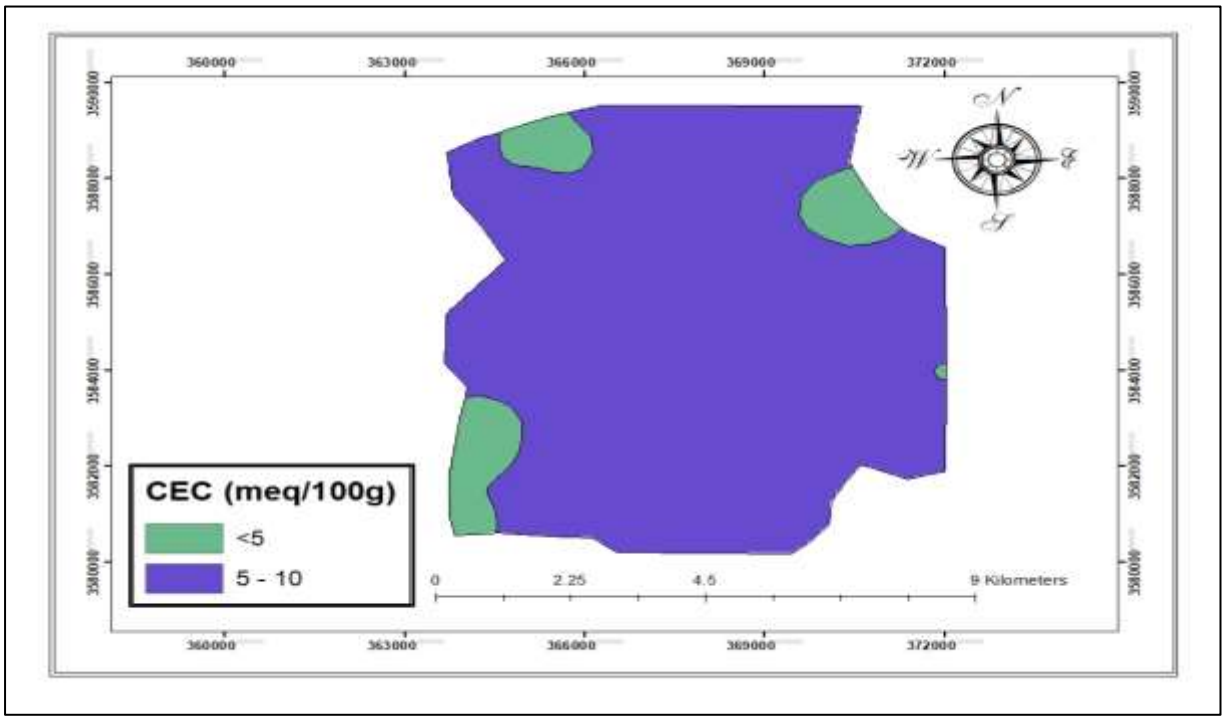

Figure 14. Spatial distribution of electrical conductivity in the study area

Carbonate minerals

The results in Table (3) show that the calcium carbonate content in the pedons of the study area ranged between 2.5 and 48.0 g kg^{-1}. A characteristic feature of Iraqi soils is their high carbonate content, which is attributed to the low leaching rates caused by limited rainfall, and geographic information systems (GIS) were employed to detect spatial variability in carbonate mineral salinity and to map the spatial distribution of some characteristics of the soils in the study area (Lotfy, 2022; Akram and Hamad, 2024).

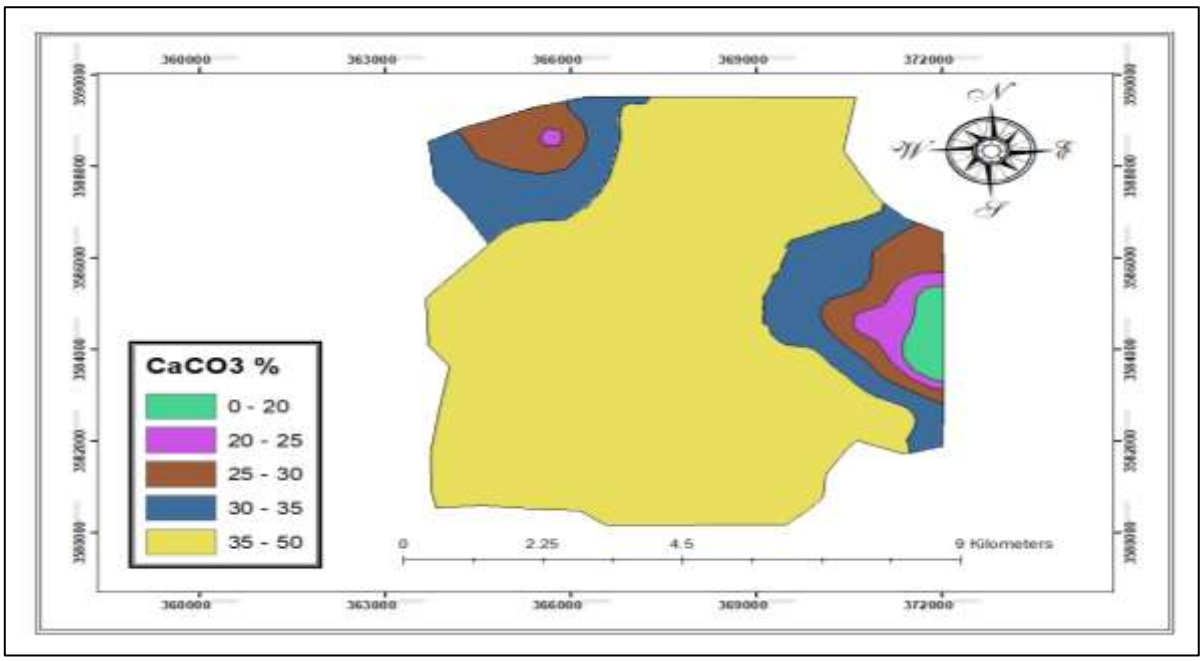

Figure 15. Spatial distribution of soil carbonate minerals in the study area

Gypsum ($CaSO_4$)

Table 2 shows that the gypsum content in the horizons of the pedons in the study area was relatively low, ranging between 0.01 and 41.82 g kg^{-1}. This reduction is attributed to the high calcium carbonate content. The results also revealed that the vertical and horizontal distributions of gypsum were irregular, with values generally increasing with depth. The lowest contents were recorded in the surface horizons of pedons 1, 3, 8, and 9. In addition, the surface horizon of pedon 7 was completely devoid of gypsum

(nil). The observed pattern indicates that as the calcium carbonate content increases, the gypsum content decreases because of competition between sulfate and carbonate ions for calcium, which determines whether gypsum or calcite is formed.

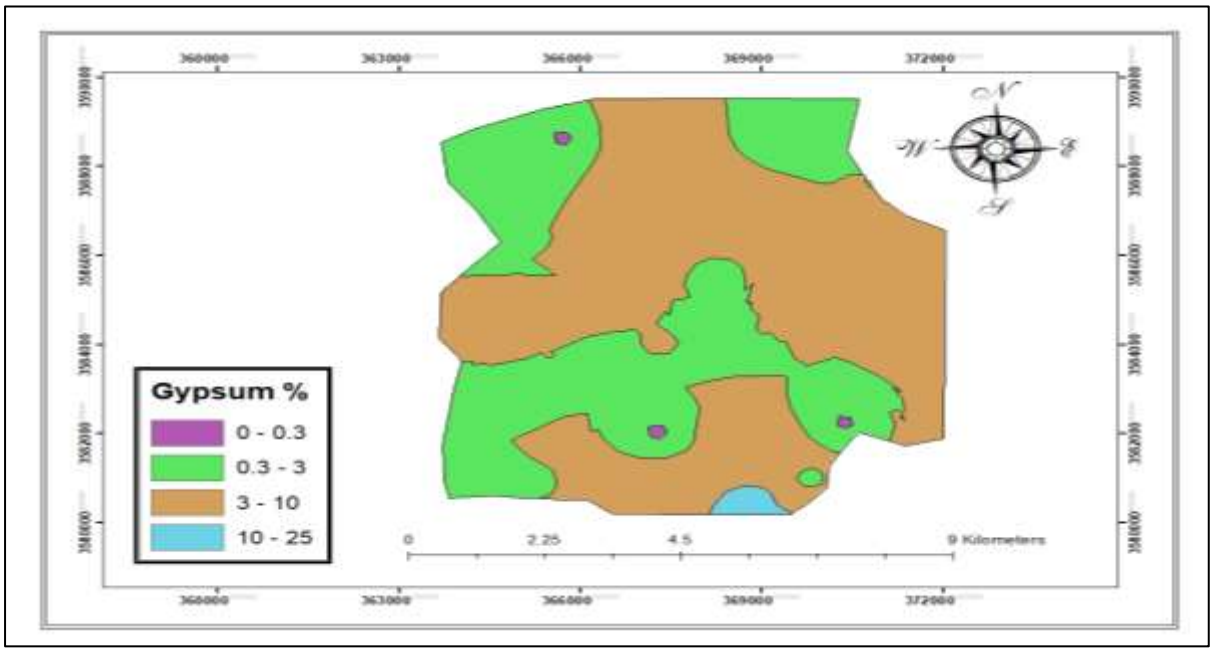

Figure 16. Spatial distribution of gypsum in the soils of the study area

Organic matter (OM)

As shown in Table (2), the organic matter content was very low across all the pedons in the study area, reaching only 0.03 g kg^{-1}. This reduction is attributed to the abandonment of land by farmers, combined with high temperatures and low winter rainfall. Under such conditions, organic matter cannot form or accumulate in significant amounts. These factors contribute to the depletion of organic matter, which in turn reduces soil productivity and biological diversity (Anbar and Hamad, 2025).

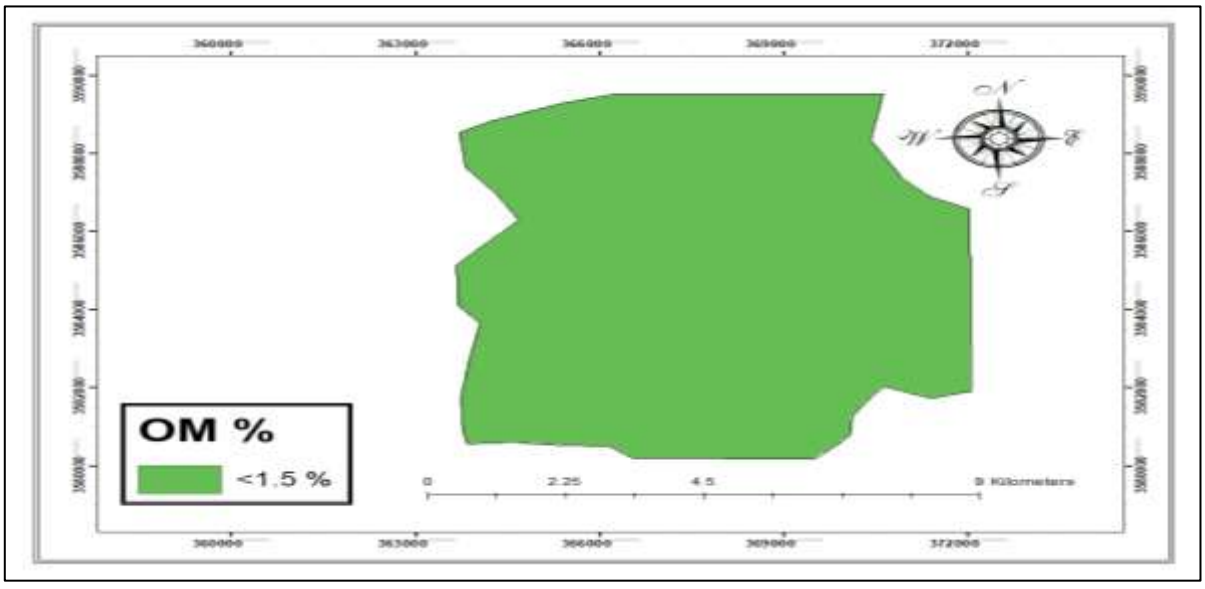

Figure 17. Spatial distribution of soil organic matter in the study area

Table 2. Some chemical properties of the pedons in the study area

Pedon	Horizon	Depth	P	EC	ESP	CEC	$CaCO_3$	$CaSO_4$	O.M
				dSm^{-1}		$Cmol_c kg^{-1}$ Soil	%	%	%
1	Ap	0-25	8.3	0.96	6.4	4.6	24.0	0.09	0.44
	C_y	25-55	7.2	2.76	6.6	4.8	27.5	5.68	0.19
	C_{ky}	55-80	7.9	2.87	6.4	5.7	30.0	30.96	0.28

	C_1	80-100	8.4	3.11	6.4	5.4	25.5	24.89	0.12
2	Ap	0-20	7.9	1.48	6.5	5.1	38.0	9.91	0.44
	C_{y1}	20-50	8.0	3.0	6.4	4.1	12.5	29.42	0.06
	Cy_2	50-90	7.1	10.5	7.6	3.8	14.0	29.28	0.22
	Cy_3	90-120	8.0	13.3	9.5	3.2	17.5	22.45	0.09
3	Ap	0-25	7.2	4.48	8.1	7.14	44.0	1.07	0.72
	C_1	25-50	8.1	9.6	8,1	3.8	11.0	1.88	0.25
	C_{ky}	50-80	8.4	3.8	6,6	4.8	27.0	16.21	0.28
	C_2	80-120	7.0	2.87	7,3	4.82	7.5	5.98	0.34
4	Ap	0-15	7.0	3.59	7.4	7.9	39.5	2.25	0.28
	Cy_1	15-40	7.4	2.75	7,3	6.08	20.0	27.41	0.38
	Cy_2	40-90	7.4	2.68	7.2	6.4	22.5	23.95	0.22
	Cy_3	90-125	7.4	2.65	7.2	8.2	31.5	13.98	0.28
5	Ap	0-20	8.0	2.5	6.6	8.5	41.0	2.42	0.38
	Cy_1	20-50	7.6	2.73	7,2	9.1	13.0	41.82	0.41
	Cy_2	50-80	7.6	2.67	7.1	7.5	19.5	27.41	0.03
	Cy_3	80-120	7.3	2.99	6,9	8.3	17.5	26.55	0.28
6	Ap	0-20	7.4	4.63	8.3	4.84	3.7	5.16	0.79
	Cy_1	20-40	7.2	15.7	20.1	6.96	4.5	11.29	0.28
	Cy_2	40-80	7.3	25.8	26.4	5.46	17.5	10.20	0.88
	C_1	80-120	7.4	19.2	22.2	4.23	2.5	6.22	0.72
7	Ap	0-17	7.9	0.46	6.5	4.45	42.5	Nill	0.!50
	C_1	17-50	7.9	0.661	6.6	4.63	4.3	0.01	0.12
	C_y	50-80	7.4	2.54	6.6	4.91	3.6	15.77	0.34
	C_2	80-100	7.6	2.6	6.6	3.36	40.5	3.63	0.12
8	Ap	0-30	7.3	0.909	6.4	9.36	43.5	0.02	0.19
	C_y	30-60	7.7	3.68	7.1	4.68	14.5	20.02	0.03
	C_{ky}	60-90	7.7	2.9	6.6	7.50	25.5	11.73	0.41
	C_k	90-120	7.2	3.03	6.4	6.42	44.5	2.73	0.28
9	Ap	0-15	7.6	2.54	6.5	4.73	43.0	1.51	0.38
	C_{k1}	15-40	7.4	0.68	7.0	5.25	46.5	0.01	0.34
	Ck_2	40-70	7.3	2.58	6.4	7.43	43.5	3.99	0.19
	Ck_3	70-115	7.5	2.73	6.6	4.01	40.0	5.05	0.19
10	Ap	0-17	7.6	2.69	6.5	5.0	48.0	1.99	0.19
	Ck	17-40	7.8	6.48	7.2	7.0	46.0	0.97	0.25
	C_{ky1}	40-80	7.5	51.6	19.2	5.4	34.5	13.16	0.09
	C_{ky2}	80-110	7.8	14.7	17.2	6.42	25.5	11.88	0.09
11	Ap	0-30	7.6	0.60	6.4	7.32	48.0	0.02	0.57
	C_{K1}	30-60	7.0	3.3	8.8	7.23	47.0	1.14	0.03
	C_{K2}	60-83	7.2	7.0	9.4	6.24	47.5	2.72	0.22
	C_{K3}	83-110	7.2	5.2	8.3	5.14	46.5	0.76	0.38
12	Ap	0-20	7.3	2.7	6.4	7.07	35.0	20.97	0.15
	CK1	20-50	7.5	3.3	6.7	5.94	34.5	18.14	0.34
	C_{KY2}	50-80	7.7	2.9	6.5	6.03	36.0	16.57	0.15
	C_{KY3}	80-110	7.3	6.4	9.9	6.0	37.0	12.21	0.12

Producing a Soil Series Map Using the Inverse Distance Weighted (IDW) Method

The series level is among the most important and prominent classification levels used, and the use of the inverse distance weighted (IDW) method for soil management relies upon the agricultural aspect. Its role involves storing large amounts of data that benefit the soil for agricultural purposes and preparing all necessary administrative requirements to achieve high productivity. With the advancement of technology in the world of techniques, where remote sensing technology, geographic information systems (GIS), and drone aircraft in imaging operations have emerged, it has become easy to isolate image units and produce maps using the IDW method through the ArcGIS program, utilizing the average reflectance values of the aerial image taken for the locations of the soil series. This has contributed to soil surveying processes with high accuracy and low costs.

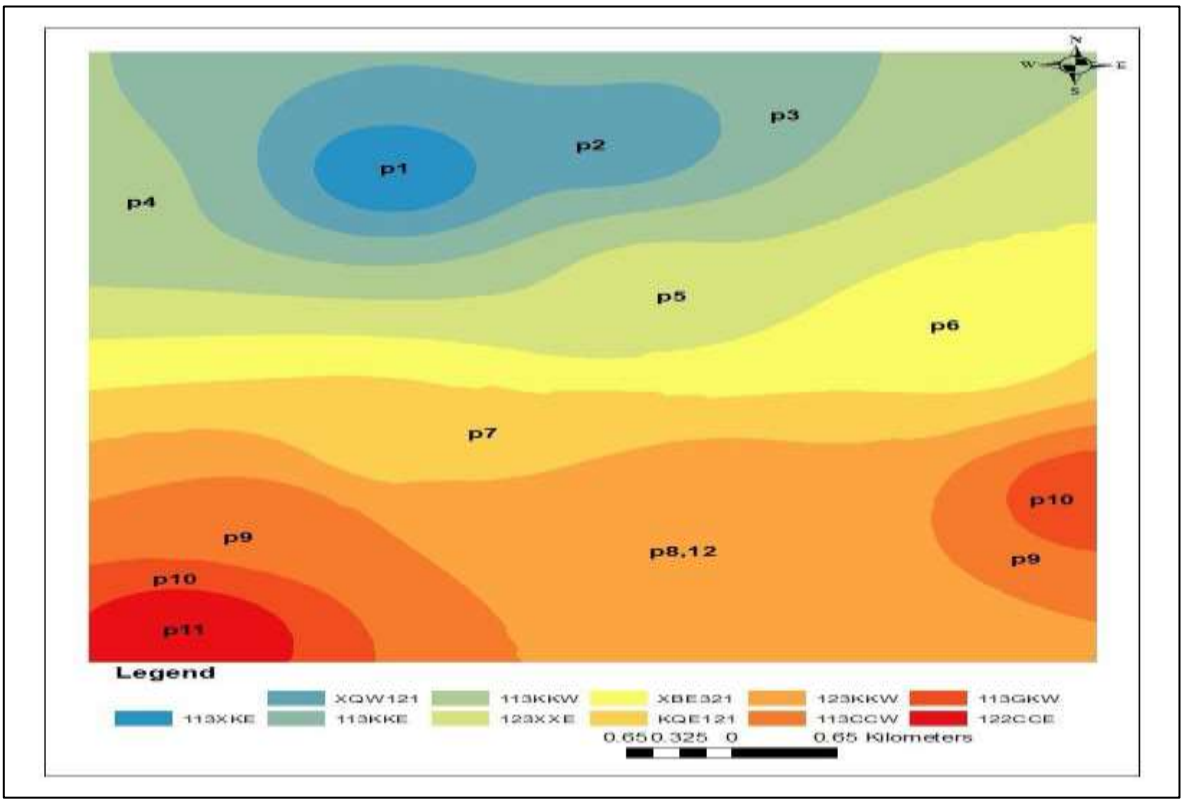

Figure 18. Soil series map of the study area using the IDW method

Cartographic analysis of soil series

The results presented in Figure (18) indicate the presence of eleven soil series of varying areas and frequencies within the study area. The 123KKW series occupied the largest area, reaching 979.22883 hectares, which represents 21.559.966.7% of the total soil area of the project. It was followed by the 113KKW series with an area of 539.7499 hectares (11.868.971.3%) and the 123XXE series with 531.55297 hectares (11.703.357%). The remaining series covered smaller proportions in descending order: 1, 11, 10, 2, 9, 7, 3, and 6 within the study area. In terms of frequency, the 123KKW series appeared twice—in pedons 8 and 12. The dominance of certain soil series in terms of area is likely attributed to variations in soil texture between coarse and moderately coarse textures, as well as differences in transport intensity during sedimentation processes. Aerial photo units and soil series played essential roles in delineating the soil series map on the basis of the reflectance values. Consequently, this method contributed significantly to saving time and reducing effort in soil survey operations.

Table 3. Classification of the soils of the study area at the series and area levels

Pedon	Series	Area	Area/h	Area %
1	113XKE	815698.093764	81.56981	1.795.946.3
2	XQW121	3380726.697557	3.380.7267	7.443.444.58
3	113KKE	4754188.284042	475.41883	10.467.435
4	113KKW	5390749.865833	539.7499	11.868.971.3
5	123 XXE	5315529.694669	531.55297	11.703.357
6	XBE 321	5179631.478124	517.96315	11.404.145.8
7	KQE121	4445960.241918	444.59602	9.788.800.23
8	123KKW	9792288.262794	979.22883	21.559.966.7
9	113CCW	3972425.191013	397.24252	8.746.204.41
10	113GKW	1412618.760212	141.26188	3.110.204.01
11	122CCE	959030.099484	95.90301	2.111.524.54

The data in Table 4 indicate that all the pedons are assigned to the Aridisols order, as expected, according to the climate of those regions and the existence of calcic and gypsic horizons. Two suborders are recognized within this order: Gypsids and Calcids. Three major subgroups are also recognized:

Haplocalcids, Haplogypsids, and Calcigypsids.

At the level of a subgroup, five subgroups are identified as follows:

- Typic Haplogypsids are represented by pedons 2, 4, 5.7, and 8.
- Lithic Haplogypsids, depicted by pedon 6
- Lithic Calcigypsids, represented by pedon 10.
- Typic Calcigypsids, represented by pedons 1, 3, and 12.
- Typic Haplogypsids, represented by pedons 9 and 11.

Table 4. Classification of the study soils according to the U.S. Soil Taxonomy (2014) at the subgroup level and to the series level according to Al-Akaidi (1981).

Pedon	Series	Sub group	Grate. group	S. ora.	Ora.
2	XQW121	Typic Haplogypsids	Haplo gypsids	Gypsids	Aridi Sols
4	113KKW	Typic Haplogypsids			
5	123 XXE	Typic Haplogypsids			
7	KQE121	Typic Haplogypsids			
8	123KKW	Typic Haplogypsids			
6	XBE 321	Lithic Haplogypsids			
10	113GKW	Lithic Calcigypsids	Calcigypsids		
1	113XKE	Typic Calcigypsids			
12	123KKW	Typic Calcigypsids			
3	113KKE	Typic Calcigypsids			
9	113CCW	Typic Haplogypsids	Haplo calcids	Calcids	
11	122CCE	Typic Haplogypsids			

Conclusion

The results of this study demonstrate that unmanned aerial vehicle (UAV) imagery is a highly efficient and accurate tool for soil survey and classification in desert environments. Compared with the Sentinel-2 satellite imagery (10 × 10 m), the superior spatial resolution of the UAV imagery (0.04 × 0.04 m) enabled detailed discrimination of soil surface features and facilitated accurate identification of twelve soil series, all of which belong to the Aridisols order.

The integration of UAV data with geometric correction, digital image processing, and field verification significantly enhanced mapping accuracy while reducing survey time, labor requirements, and overall costs. In comparison, the ability of medium-resolution satellite imagery to capture fine-scale soil variability was limited because of pixel mixing effects.

Overall, UAV-based remote sensing provides a reliable, flexible, and cost-effective approach for detailed soil mapping and sustainable land management in arid and semiarid regions, such as the western desert of Karbala Governorate. The methodology presented in this study can be effectively applied to similar desert environments to support smart agriculture and land resource planning.

Ethical and Environmental Considerations

This study was conducted in accordance with applicable national and international ethical standards. No ethical approval was needed, as the research did not involve experiments on humans or animals.

Conflict of Interest

The authors declare that there are no conflicts of interest regarding the publication of this manuscript.

Data availability

All the data generated or analysed during this study are included in this published article.

Human and Animal Rights

This research did not involve human participants or animals; therefore, no ethical approval or consent procedures were applicable.

References

1. Abbas, M. S., & Wahib, Q. A. R. (2022). Spatial variations of some soil chemical and fertility characteristics in a hydrological succession in grain-growing areas in the Najaf and Diwaniyah governorates. *Iraqi Journal of Soil Science*, 20(1), 118–129. Available from: https://search.emarefa.net/detail/BIM-1309794
2. Abdel-Qader, I., Al-Mahdi, H., & Hassan, R. (2023). Assessment of soil salinity using remote sensing spectral indices in arid regions. *Environmental Monitoring and Assessment*, 195, 112. https://doi.org/10.1007/s10661-023-11025-6
3. Abdel-Qader, M. R., Raad, A. K. H., & Ahmed, B. K. (2023). Preparing soil maps in Mansourieh City–Diyala–Iraq using remote sensing and GIS. *AIP Conference Proceedings*, 2839, 030001. https://doi.org/10.1063/5.0154026
4. Abdelelah, L. A., & Wheib, K. A. (2025). Using UAV imagery vegetation indices combination in delineation of soil map units. *Iraqi Journal of Agricultural Sciences*, 56(Special Issue), 132–147. https://doi.org/10.36103/avh6v615
5. Abdulsada, A. R. (2020). Evaluation of desert land resources using GIS and remote sensing techniques. *Iraqi Journal of Agricultural Sciences*, 51(3), 789–802.
6. Abdulsada, R. S., & Hamad, A. I. (2020). Evaluation of chemical soil degradation in the Musyab project using fuzzy logic in geographic information system. *Iraqi Journal of Agricultural Sciences*, 51(Special Issue), 53–60. https://doi.org/10.36103/ijas.v51iSpecial.88217
7. Akram, A. A., & Hamad, A. I. (2024). Spatial variability of land surface heat emissions in determining desert soil characteristics in Al-Samawah Desert using GIS. *Iraqi Journal of Agricultural Sciences*, 55(5), 1637–1649.
8. Al-Hemoud, A., Al-Dousari, A., Al-Dashti, H., Petrov, P., Al-Saleh, A., Al-Khafaji, S., et al. (2020). Sand and dust storm trajectories from the Mesopotamian flood plain in Iraq to Kuwait. *Science of the Total Environment*, 710, 136291. https://doi.org/10.1016/j.scitotenv.2019.136291
9. Al-Jubouri, A. K., & Wheib, K. A. (2020). Effect of soil salinity on spectral reflectance of red and near-infrared wavelengths in Al-Salamiyat project. *Plant Archives*, 20, 1359–1365.
10. Al-Jubouri, A. M., Hishem, S. M., Suliman, A. A., & El-Desouki, S. A. (2023). Survey and classification of soils in Sheikh Saad subdistrict, Wasit Governorate, Iraq using UAV imagery. *IOP Conference Series: Earth and Environmental Science*, 1252(1), 012056. https://doi.org/10.1088/1755-1315/1252/1/012056
11. Al-Sarajati, H. A. I. (2020). *Relationship between spectral signature and Aridisols of Al-Najaf Sea area using different remotely sensed data* (PhD Dissertation). College of Agricultural Engineering Sciences, University of Baghdad, Iraq.
12. Anbar, A. R., & Hamad, I. A. (2025). Evaluation of land suitability for irrigated wheat cultivation using two different methods in northern Ali Al-Gharbi district. *Iraqi Journal of Agricultural Sciences*, 56(Special Issue), 148–161. https://doi.org/10.36103/bhqh51940
13. Chapman, H. D. (1965). Cation exchange capacity. In C. A. Black (Ed.), *Methods of Soil Analysis* (pp. 891–901). ASA, Madison, WI, USA.
14. Dawod, G. M. (2013). *An introduction to aerial photographs and satellite images*. Makkah, Saudi Arabia. https://doi.org/10.13140/RG.2.1.4614.5764
15. Gee, G. W., & Bauder, J. W. (1986). Particle-size analysis. In A. Klute (Ed.), *Methods of Soil Analysis, Part 1* (pp. 383–411). ASA and SSSA, Madison, WI, USA.
16. Hamad, W. J., & Suliman, A. A. (2021). Use of aerial images taken by drones for soil survey of the Akkarkof area northwest of Baghdad, Iraq. *Plant Archives*, 21(Suppl. 1), 1388–1394.
17. Hamad, S. A., & Suliman, A. A. (2021). Effect of UAV flight altitude on spatial resolution and classification accuracy. *Remote Sensing Letters*, 12(5), 503–512. https://doi.org/10.1080/2150704X.2021.1895582
18. Jasim, A., Zaeen, A., Sharma, L. K., Bali, S. K., Wang, C., Buzza, A., et al. (2020). Predicting phosphorus and potato yield using active and passive sensors. *Agriculture*, 10(11), 564. https://doi.org/10.3390/agriculture10110564
19. Lekka, C., Spyridon, E. D., George, P. P., & Christos, C. (2024). Mapping and monitoring of salt-affected soils: The contribution of geoinformation. In *Remote Sensing in Precision Agriculture* (pp. 71–91). Elsevier.
20. Lillesand, T. M., Kiefer, R. W., & Chipman, J. W. (2015). *Remote sensing and image interpretation* (7th ed.). John Wiley & Sons, New York, USA.
21. Lotfy, K. E. (2022). Modern and future trends in geographic information systems. *Journal of Faculty of Arts Research, Menoufia University*, 33(131), 3–35.

https://doi.org/10.21608/sjam.2022.158351.1686
22.Mohammed, R. J., & Suliman, A. A. (2023). Land suitability assessment for wheat production using analytical hierarchy process and parametric method in Babylon Province. *Journal of Ecological Engineering*, 24(7), 75–87. https://doi.org/10.12911/22998993/163349
23.Nelson, D. W., & Sommers, L. E. (1982). Total carbon, organic carbon, and organic matter. In A. L. Page et al. (Eds.), *Methods of Soil Analysis, Part 2* (pp. 539–579). ASA and SSSA, Madison, WI, USA.
24.Pessoa, L. G., Freire, M. B. D. S., Green, C. H., Miranda, M. F., Filho, J. C. A., & Pessoa, W. R. (2022). Assessment of soil salinity status under different land-use conditions in the semiarid region of northeastern Brazil. *Ecological Indicators*, 141, 109139.
https://doi.org/10.1016/j.ecolind.2022.109139
25.Qubaa, A. R., Hamden, A. N., & Al-Jawadi, T. A. (2021). Morphology detection in archaeological ancient sites using UAV data and GIS techniques. *Iraqi Journal of Science*, 62(SI), 1–10. https://doi.org/10.24996/ijs.2021.62.11(SI).35
26.Richards, L. A. (1954). *Diagnosis and improvement of saline and alkali soils*. USDA Handbook No. 60, Washington, DC, USA.
27.Sadiq, T. (2023). Machine learning and GIS techniques in flood risk mapping: The case of M'sila. *Journal of Architecture and Child's Environment*, 8(2), 4–14.
28.Soil Survey Staff. (2014). *Keys to Soil Taxonomy* (12th ed.). USDA-NRCS, Washington, DC, USA.
29.Soil Survey Staff. (2017). *Soil Survey Manual*. USDA Handbook No. 18, Washington, DC, USA.
30.Tamouridou, A. A., Alexandridis, T. K., Pantazi, X. E., Lagopodi, A. L., Kashefi, J., & Moshou, D. (2017). Evaluation of UAV imagery for mapping weed patches. *International Journal of Remote Sensing*, 38(8–10), 2246–2259. https://doi.org/10.1080/01431161.2016.1264026
31.Torres-Sánchez, J., Peña, J. M., de Castro, A. I., & López-Granados, F. (2014). Multitemporal mapping of vegetation fraction in early-season wheat fields using UAV images. *Computers and Electronics in Agriculture*, 103, 104–113. https://doi.org/10.1016/j.compag.2014.02.009
32.Wadod, M. M., & Mohammed, F. G. (2023). Review on drone application methodologies in precision agriculture. *IOP Conference Series: Earth and Environmental Science*, 1202(1), 012001. https://doi.org/10.1088/1755-1315/1202/1/012001
33.Wheib, K. A., Ati, A. S., & Aljabar, S. A. (2024). Assessment of UAV imagery in monitoring wheat canopy cover in Diwaniya Governorate, Iraq. *Iraqi Journal of Agricultural Sciences*.
34.Wijayanto, A. K., Junaedi, A., Sujaswara, A. A., Khamid, M. B., Prasetyo, L. B., Hongo, C., et al. (2023). Machine learning for precise rice variety classification using UAV-based multispectral sensing. *AgriEngineering*, 5(4), 2000–2019. https://doi.org/10.3390/agriengineering5040117